Electronic Supplementary Material (ESI) for Journal of Materials Chemistry A.

A novel solid-state synthesis route for the high voltage $Na_3V_2(PO_4)_2F_{3-2y}O_{2y}$ cathode materials for Na-ion batteries

Supplementary information

Mainul Akhtar,[a,b] *Hafssa Arraghraghi,*[a,b] *Sylvia Kunz,*[a,b] *Qingsong Wang,*[a,b] *and Matteo Bianchini* [a,b,*]

[a] Department of Chemistry, Universität Bayreuth, Universitätsstrasse 30, 95447 Bayreuth Germany

[b] Bavarian Center for Battery Technology (BayBatt), Universität Bayreuth, Weiherstrasse 26 95448 Bayreuth Germany

*E-Mail: matteo.bianchini@uni-bayreuth.de

Pages: S1-S14

Table S1: ICSD entries for the structures used for DFT calculations.

Material	ICSD code
NaF	262837
$VOPO_4$	9413
VPO_4	36521
Na_2CO_3	12168
$(VO)_2P_2O_7$	88661
NVPF	194603
$NVPF_2O$	Own data – XRD refinement
$NVPFO_2$	194604

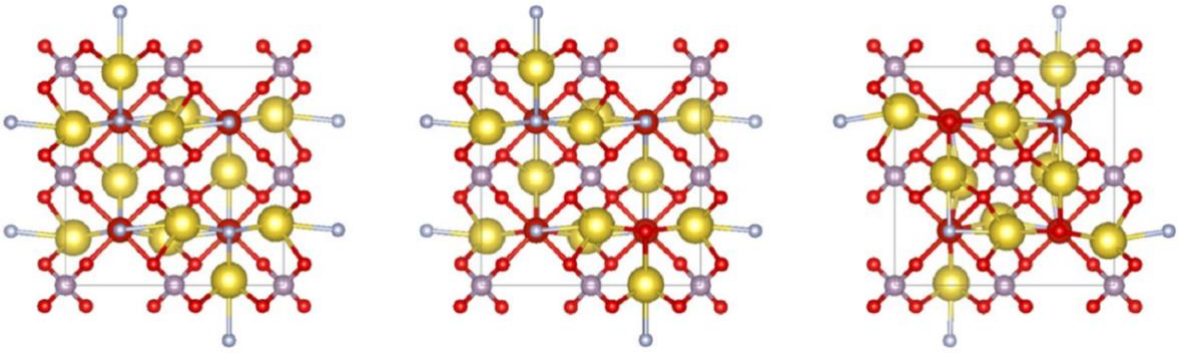

Figure S1 Crystal structures of $NVPF_{3-2y}O_{2y}$ used for DFT calculations: (left) NVPF, (middle) $NVPF_2O$, (right) $NVPFO_2$. The structures are seen in the a-b crystallographic plane (c axis pointing out of the paper). The spheres yellow, purple, light red, dark red and blue represent Na, P, O, V and F, respectively.

Table S2: Structural parameters obtained from Rietveld refinement of NVPF.

NVPF						
S.G.: *Amam*; Z = 4						R_{Bragg} = 4.82%
a = 9.0357(1) Å; *b* = 9.0475(1) Å; *c* = 10.74322(8) Å; *V* = 878.27(1) Å^3; *V/Z* = 219.568(4) Å^3						R_{wp} = 12.8%
						χ^2 = 14.0
		atomic position				
atoms	Wyckoff position	*x/a*	*y/b*	*z/c*	occ	B_{iso}
V	8 g	0.25	0.2534(3)	0.18536(9)	1	0.80(1)
P	8 e	0.00	0.000	0.2453(4)	1	0.84(3)
O1	16 h	0.0973(6)	0.0954(7)	0.1601(4)	1	1.19(2)
O2	16 h	0.0916(6)	0.4015(7)	0.1681(4)	1	0.7(1)
F1	4 c	0.025	0.248(1)	0.000	1	0.48(7)
F2	8 g	0.025	0.7571(8)	0.1343(2)	1	1.92(7)
Na1	4 c	0.075	0.019(1)	0.0000	1	4.8(3)
Na2	8 f	0.5330(8)	0.2851(6)	0.0000	0.72(1)	1.8(2)
Na3	8 f	0.864(1)	0.412(1)	0.0000	0.31(1)	3.3(5)

Table S3: Structural parameters obtained from Rietveld refinement of $NVPF_2O$ prepared from pyrophosphate source.

$NVPF_2O$						
S.G.: *$P4_2/mnm$;* Z = 4						R_{Bragg} = 5.79%
a = *b* = 9.04091(6) Å; *c* = 10.6699(1) Å; *V* = 872.13(1) $Å^3$; *V/Z* = 218.034(3) $Å^3$						R_{wp} = 13.3%
						χ^2 = 39.4
		atomic position				
atoms	Wyckoff position	*x/a*	*y/b*	*z/c*	occ	B_{iso}
V	8 j	0.2487(3)	0.2487(3)	0.1922(1)	1	0.99(2)
P1	4 d	0	0.5	0.25	1	1.3(2)
P2	4 e	0	0	0.2563(6)	1	0.6(1)
O1	16 k	0.0954(7)	0.4069(7)	0.1637(6)	1	0.8(2)
O2	8 j	0.0948(7)	0.0948(7)	0.156(1)	1	1.0(3)
O3	8 j	0.4004(7)	0.4004(7)	0.170(1)	1	1.0(3)
O4	8 j	0.2475(9)	0.2475(9)	0.3582(3)	0.5	2.06(8)
F1	8 j	0.2475(9)	0.2475(9)	0.3582(3)	0.5	2.06(8)
F2	4 f	0.2490(9)	0.2490(9)	0	1	0.72(8)
Na1	8 i	0.5156(7)	0.2360(9)	0	0.8(1)	2.0(1)
Na2	8 i	0.8061(8)	0.037(1)	0	0.7(1)	5.9(4)

Table S4: Structural parameters obtained from Rietveld refinement of $NVPFO_2$ prepared from pyrophosphate source.

$NVPFO_2$						
S.G.: $P4_2/mnm$; Z = 4						R_{Bragg} = 5.05%
$a = b$ = 9.03231(5) Å; c = 10.61917(7) Å; V = 866.339(9) Å^3; V/Z = 216.584(2) Å^3						R_{wp} = 12.6%
						χ^2 = 53.8
		atomic position				
atoms	Wyckoff position	*x/a*	*y/b*	*z/c*	occ	B_{iso}
V	8 j	0.2483(2)	0.2483(2)	0.19913(8)	1	0.78(1)
P1	4 d	0	0.5	0.25	1	0.8(2)
P2	4 e	0	0	0.2532(5)	1	0.7(2)
O1	16 k	0.0968(7)	0.4059(7)	0.1629(7)	1	0.8(2)
O2	8 j	0.0954(7)	0.0954(7)	0.154(1)	1	0.6(2)
O3	8 j	0.4017(7)	0.40174(6)	0.17109(1)	1	1.4(3)
O4	8 j	0.2483(7)	0.2483(7)	0.3508(3)	1	1.275(1)
F	4 f	0.2469(7)	0.2469(7)	0	1	0.61(7)
Na1	8 i	0.5120(6)	0.2331(7)	0	0.83(1)	1.12(1)
Na2	8 i	0.7982(8)	0.025(1)	0	0.69(1)	5.57(4)

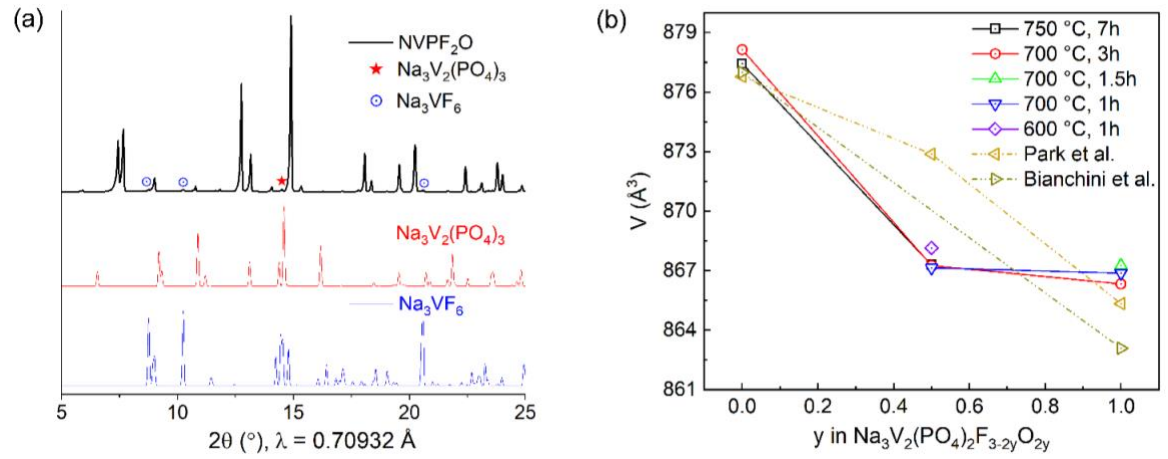

Figure S2 (a) Powder X-ray diffraction pattern obtained when attempting to prepare $NVPF_2O$ from $VOPO_4$ source. The $Na_3V_2(PO_4)_3$ and Na_3VF_6 impurities are highlighted by red star and blue circled dot symbols, respectively. The red and blue indexations below the figure are for $Na_3V_2(PO_4)_3$ and Na_3VF_6. (b) Lattice volume changes as a function of oxygen substitution for fluorine in $NVPF_{3-2y}O_{2y}$ at various temperatures and times.

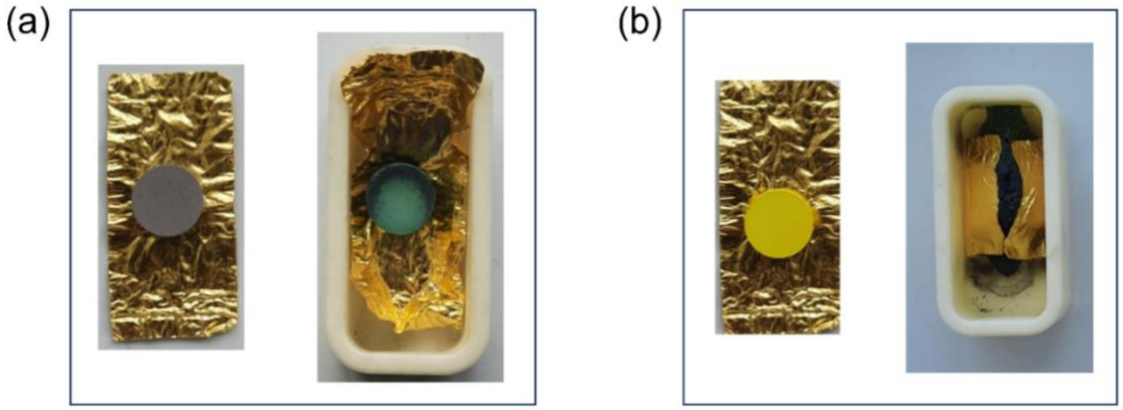

Figure S3 (a) The photograph of the pellets before and after the reaction (heat treated at 700 °C for 1 h) for $NVPFO_2$ from $(VO)_2P_2O_7$ source. (b) The porous and significantly expanded $NVPFO_2$ sample obtained from synthesis reaction of $VOPO_4$ source after heat treated at 700 °C for 1 h.

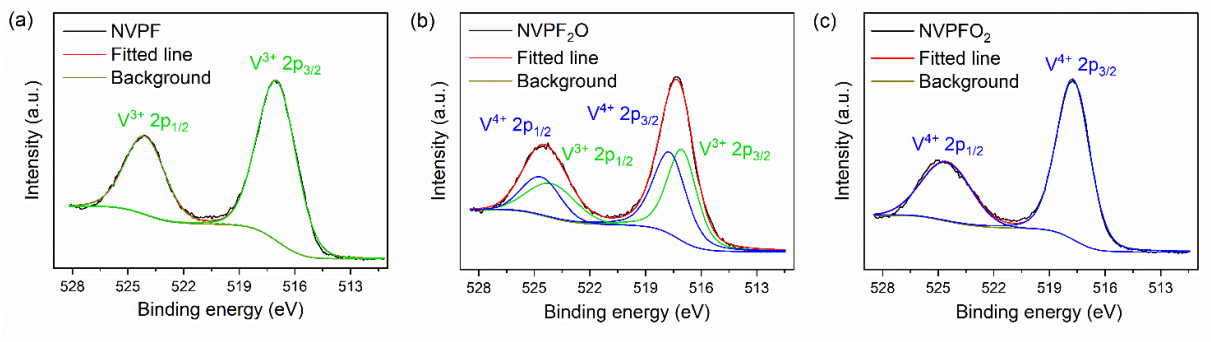

Figure S4 Characterization of the oxidation state of $NVPF_{3-2y}O_{2y}$ (y = 0, 0.5, 1) samples. (a) XPS spectra of V^{3+} $2p_{3/2}$ and V^{3+} $2p_{1/2}$ energy levels in NVPF sample. (b) The appearance of both V^{3+} 2p and V^{4+} 2p modes in $NVPF_2O$ sample. (c) XPS spectra of V^{3+} $2p_{3/2}$ and V^{3+} $2p_{1/2}$ energy levels in $NVPFO_2$ sample.

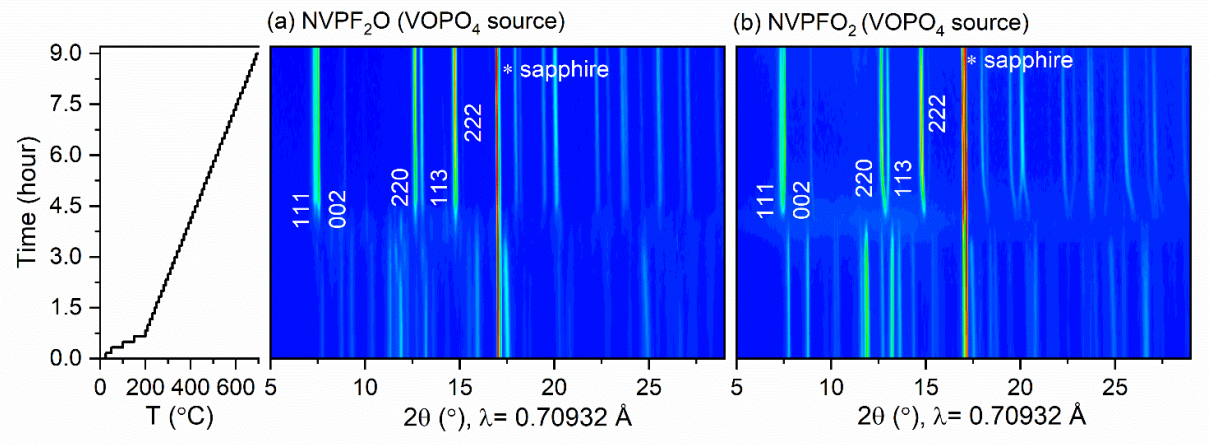

Figure S5 *In situ* high-temperature x-ray diffraction patterns (in 2D contour plots) during the solid-state synthesis of (a) $NVPF_2O$ from VPO_4, $VOPO_4$, NaF, and Na_2CO_3 (eq.4), (b) $NVPFO_2$ from $VOPO_4$, NaF, and Na_2CO_3 mixture (eq.5). (Left) Temperature ramps used over time. The temperature range was from 25 to 700 °C.

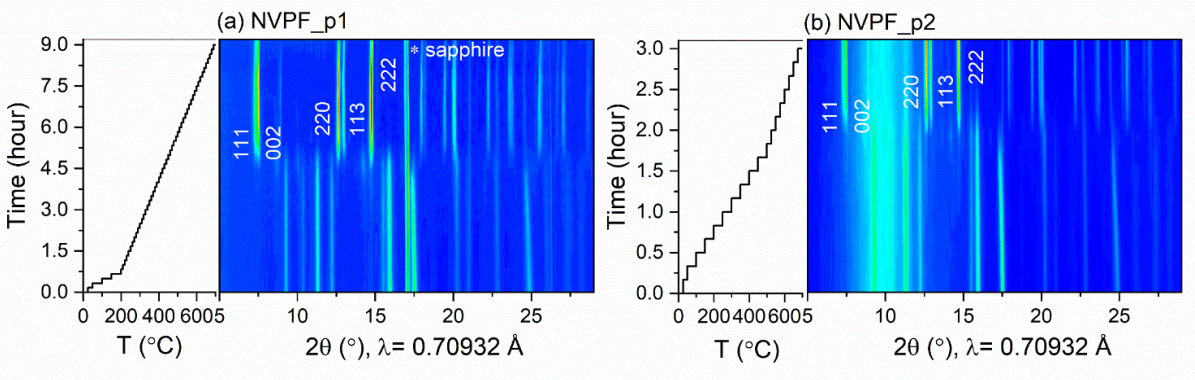

Figure S6 *In situ* high-temperature X-ray diffraction patterns (in 2D contour plots) during the solid-state synthesis of (a) NVPF_p1 from VPO_4 (V_2O_5, ThermoFisher Scientific; >99.99%) and NaF (abcr GmbH; 99.995%). (Left) Temperature ramps used over time. The temperature range was from 25 to 700 °C. (b) NVPF_p2 from VPO_4 (V_2O_5, Sigma-Aldrich *Co.* Ltd.; 99.95%) and NaF (Grüssing GmbH; >99.0%). (Left) Temperature ramps used over time. The temperature range was from 25 to 700 °C. Note that this experiment was done with quartz rather than sapphire capillary, hence the different background.

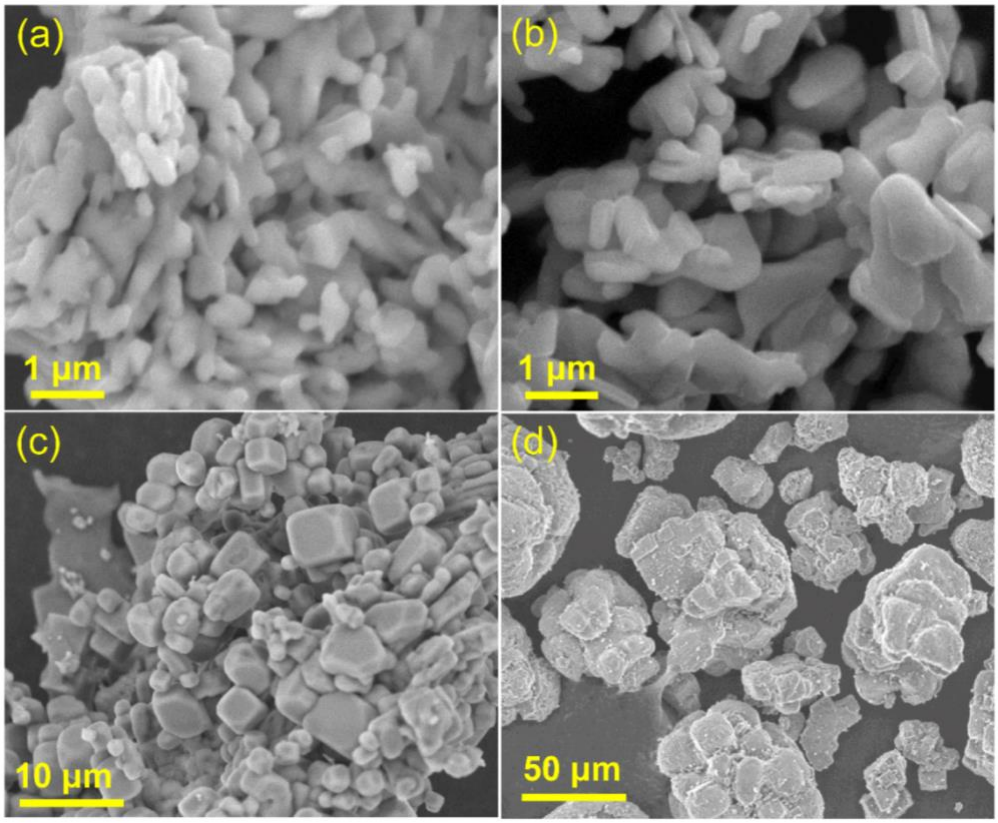

Figure S7 Scanning electron microscopy images of (a) V_2O_5, ThermoFisher Scientific; >99.99%, (b) V_2O_5, Sigma-Aldrich *Co.* Ltd.; 99.95%, (c) NaF, abcr GmbH; 99.995%, (d) NaF, Grüssing GmbH; >99.0%). The average particle sizes of V_2O_5 are in the range of 500 nm to 1 µm (ThermoFisher Scientific; >99.99%), and 1 to 2 µm (Sigma-Aldrich *Co.* Ltd.; 99.95%) for NVPF_p1 and NVPF_p2, respectively, while the corresponding values for NaF are in the range of 1 to 5 µm (abcr GmbH; 99.995%), and 20 to 25 µm (Grüssing GmbH; >99.0%) for NVPF1 and NVPF2, respectively.

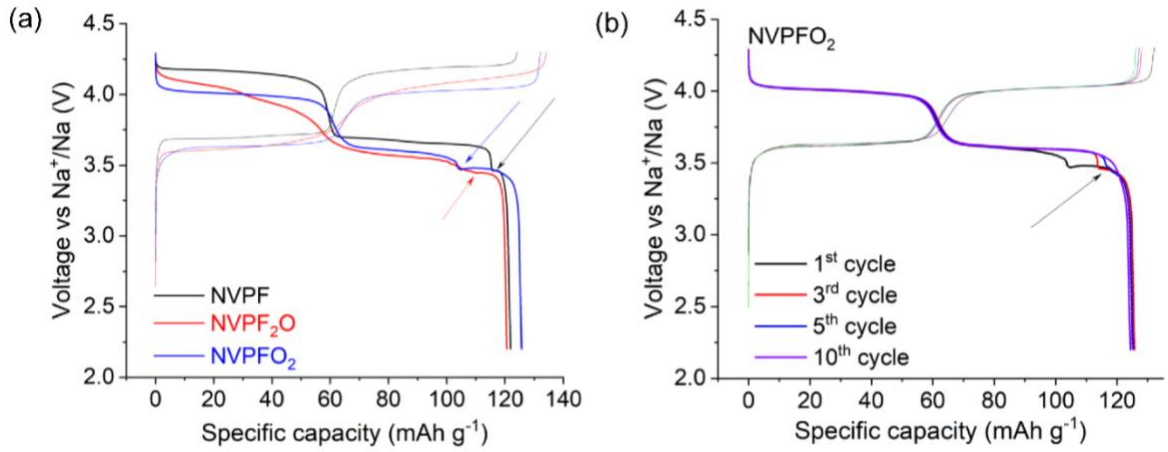

Figure S8 1st cycle charge-discharge profiles at C/20 for NVPF, $NVPF_2O$, and $NVPFO_2$ prepared from $(VO)_2P_2O_7$ source. The arrow signs around 3.4 V indicate small voltage steps during discharge. (b) 1, 3, 5 and 10th cycle charge-discharge profiles at C/20 for $NVPFO_2$ cathode. The arrow sign around 3.4 V indicates voltage step at 1, 3 and 5th cycles before completely disappearing at 10th cycle.

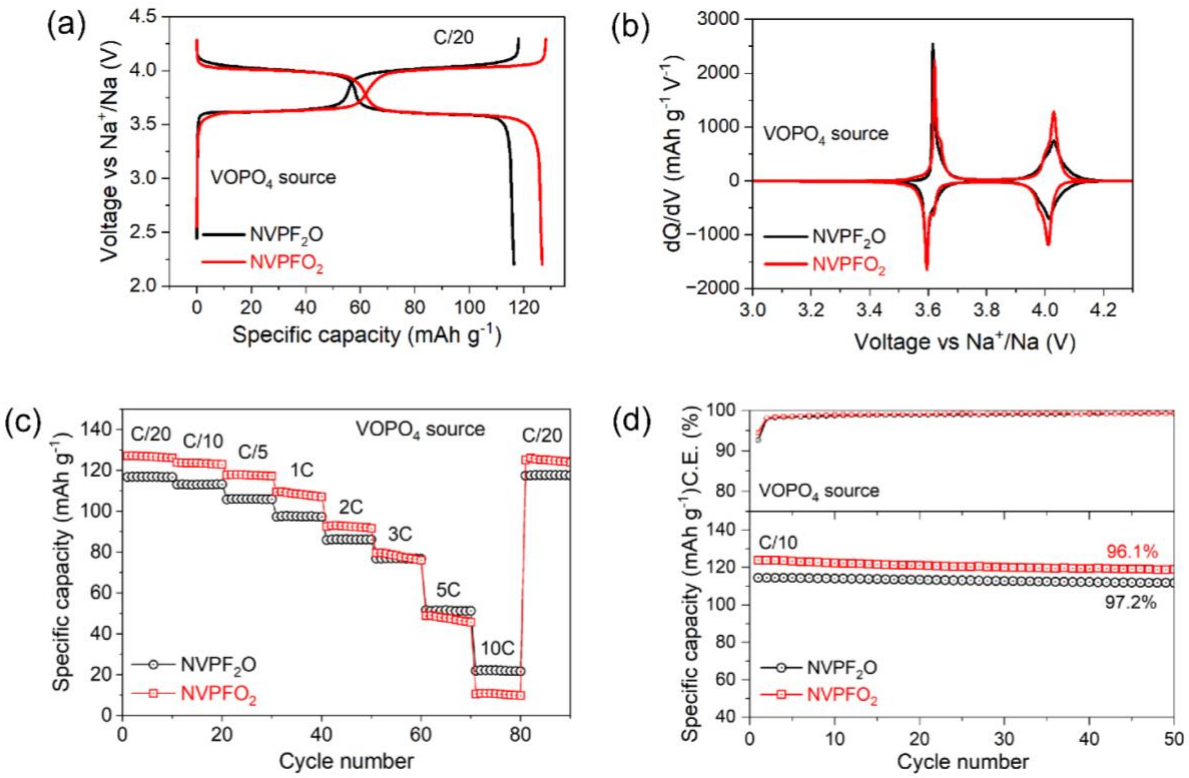

Figure S9 Electrochemical performances of $NVPF_{3-2y}O_{2y}$ (y = 0.5, 1) samples prepared from $VOPO_4$ source in 2.2-4.3 V vs Na^+/Na. (a) potential profiles for the 10th cycles at C/20 rate, (b) corresponding derivative curves for the 10th cycles, (c) rate performance, and (d) cycling performance at C/10 rate.

Note 1. Kinetic Properties: Diffusion rate from CV Rate Test

Regarding electrode kinetics, we also measured cyclic voltammetry for our electrode materials. The linear relationship between i_p and $v^{1/2}$ confirms diffusion-controlled behaviour in all the electrodes. The Na^+ diffusion coefficients (D_{Na}) are calculated using the Rendles-Sevcik equation as follows.

$$\frac{i_p}{m} = 0.4463\left(\frac{F^3}{RT}\right)^{1/2} n^{3/2} A D^{1/2} C v^{1/2} \quad \ldots \ldots \ldots (1)$$

Where i_p is the peak current, m is the active mass (3.36, 3.92, and 3.36 mg for NVPF, $NVPF_2O$, and $NVPFO_2$, respectively) F is the Faraday constant (= 96,485 C mol^{-1}), R is the gas constant (8.314 J K^{-1} mol^{-1}), T is the absolute temperature (298.15 K), n is the number of electrons per molecule involved in the reaction (=2), A is the active surface area of the cathodes (~0.50265 cm^2), C is the molar concentration of sodium ions in the electrodes (calculate as 0.022685, 0.022845, 0.022997 mol cm^{-3} for NVPF, $NVPF_2O$, and $NVPFO_2$, respectively).

The diffusion coefficients for the different electrodes are tabulated as follows.

Table S5: Diffusion coefficients extracted from the CV curves of Figure S10.

Electrode	Cathodic peaks			Anodic peaks		
	Slope		D_{avg}	Slope		D_{avg}
NVPF	0.63(1)		5.28×10^{-9}	0.59(6)		4.63×10^{-9}
$NVPF_2O$	0.56(3)	0.85(1)	1.35×10^{-8}	0.52(7)	0.60(1)	8.28×10^{-9}
$NVPFO_2$	0.74(2)	0.95(3)	1.86×10^{-8}	0.6(1)	0.80(1)	1.29×10^{-8}

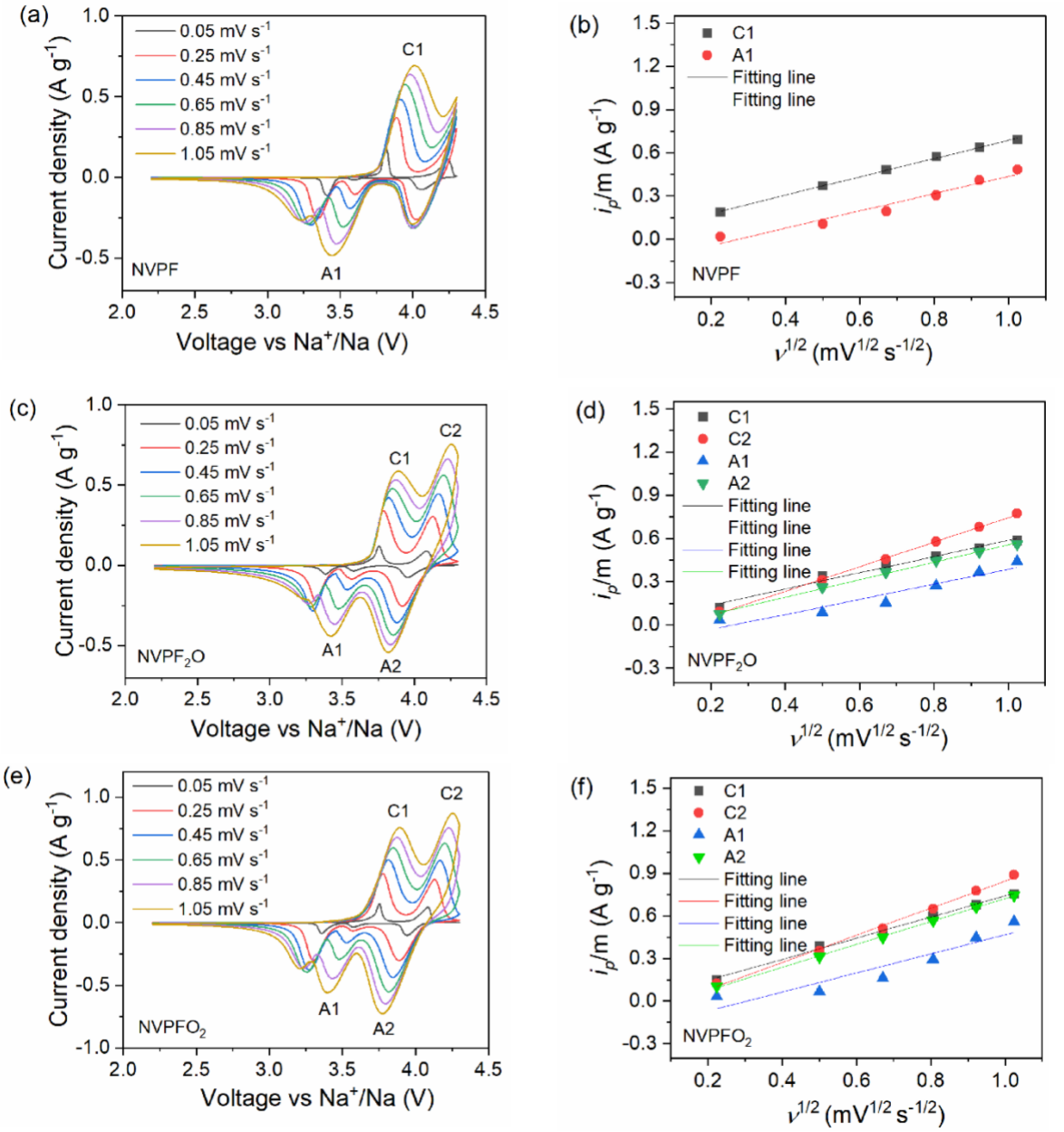

Figure S10: Cyclic voltammograms at 0.05−1.05 mV s^{-1} and corresponding peak current density (i_p/m) vs square root of the scanning rate ($v^{1/2}$): (a-b) NVPF electrode, (c-d) $NVPF_2O$ electrode and (e-f) $NVPFO_2$ electrode.

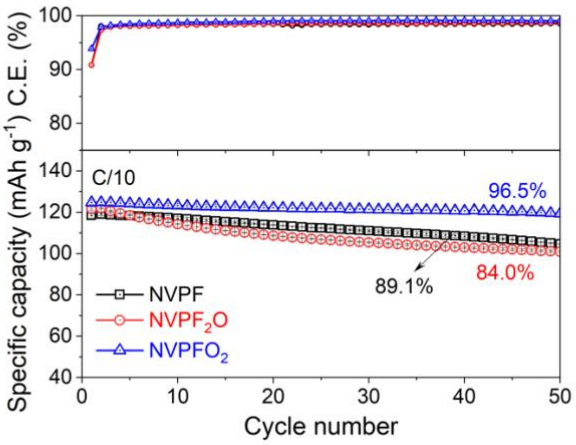

Figure S11 Electrochemical cycling performance of $NVPF_{3-2y}O_{2y}$ (y = 0, 0.5, 1) cathodes in 2.2-4.3 V vs Na^+/Na at C/10 rate. Cells were cycled in duplets.